Image Reconstruction without an Inertial Navigation System using Backprojection Autofocus for Synthetic Aperture Radar

Aron Sommer*, **Jörn Ostermann***

*Institut für Informationsverarbeitung
Appelstr. 9A, D-30167 Hannover, Germany
email: sommer@tnt.uni-hannover.de
ostermann@tnt.uni-hannover.de

Abstract: *We propose an extension of the backprojection autofocus approach to reconstruct synthetic aperture radar images with high quality from extreme coarsely measured flight paths. Usually, expensive and heavy inertial navigation systems are used to measure flight paths with high precision. Small antenna position errors up to approximately one half of the range resolution can be corrected by state-of-the-art autofocus techniques. Our approach is able to correct position errors much larger than this upper bound. For this purpose, we use the idea of the backprojection autofocus by Ash and estimate pulse-by-pulse phase errors by maximizing image sharpness. In contrast to Ash, we use additionally the estimated phase error of each considered pulse to update the aperture positions of all subsequent pulses. The evaluation of our autofocus technique using real airborne X-band data acquired in spotmode shows that the proposed method can correct antenna position errors of more than $12\,\mathrm{m}$. Thus, our algorithm allows the usage of much cheaper or even no inertial navigation systems.*

1. Introduction

Synthetic aperture radar (SAR) is a method to take radar images of the ground in all-weather conditions. A radar sensor is mounted onto an aircraft or a satellite, which flies along an almost straight flight path and illuminates the ground using electromagnetic waves. This technique enables the reconstruction of high resolution SAR images with wide-area coverage, thousands of meters away from the sensor.

However, the reconstruction of high quality SAR images is only possible, if the true flight path is exactly known. High-quality *inertial navigation systems* (INS), which could cost more than $100\,000\,\$$ and could have a weight of more than $3\,\mathrm{kg}$ [1], are typically used to measure the path accurately. Despite their high precision, these hardware systems provide antenna position errors such as drifts up to approximately $1.2\,\mathrm{cm}$ within $10\,\mathrm{s}$ [1]. The usage of these estimated flight paths instead of the true flight paths results in smeared images. As long as these drifts are less than approximately one half of the range resolution, which is roughly $12\,\mathrm{cm}$ for a typical X-band system with $640\,\mathrm{MHz}$ bandwidth [2], state-of-the-art autofocus techniques are able to correct the smearings in the resulting SAR images automatically.

State-of-the-art autofocus techniques, especially the phase gradient [3, 4] algorithm and the mapdrift autofocus [5], which have been invented for frequency-domain algorithms, require a linear platform motion. The prominent point processing [6] requires data from continuously visible prominent point targets, which can rarely be found in real SAR data. The autofocus techniques developed for the time-domain *global backprojection* (GBP) [7, 8] algorithm preserve full flexibility and no limitations on flight paths. A well known state-of-the-art time-domain autofocus algorithm is the backprojection autofocus by Ash [9], which we describe later in detail. A similar but slower approach is given by Duersch et al. [1].

However, all state-of-the-art autofocus techniques, whether they act in time- or in frequency-domain, require a rather accurately measured flight path and are only able to correct small deviations of upto approximately one half of the range resolution. Otherwise, the image quality degrades immensely.

In this paper we propose a new autofocus technique to reconstruct high quality SAR images if the antenna position errors are larger than one half of the range resolution or even if the flight direction is only available at the beginning of the flight paths. This happens if cheap INS are used instead of high quality and expensive INS sensors developed for navigation applications. Our technique uses the idea of the backprojection autofocus by Ash [9] and estimates pulse-by-pulse the phase errors by maximizing image sharpness. We propose the extension to integrate the autofocus into the GBP algorithm such that the estimated phase error of the currently considered pulse can be used to correct the aperture positions of all subsequent pulses in advance. This adjustment saves a lot of computational time.

This paper is structured as follows: The fundamentals of the used signal model are given in Sec. 2. The GBP algorithm together with the autofocus problem are formulated in Sec. 3. We also introduce the Ash autofocus, which estimates phase errors by maximizing image sharpness, in Sec. 3. Our autofocus algorithm, which integrates the Ash autofocus into the GBP algorithm and updates the flight path based on the estimated phase errors, is proposed in Sec. 4. In Sec. 5, our algorithm is evaluated using real X-band data. Finally, this paper ends with the conclusions in Sec. 6.

2. Signal Model

Let us assume that the *antenna phase center* (APC) of an airborne single-channel X-band SAR system moves along an arbitrary flight path $\boldsymbol{\gamma} : \mathcal{L} \to \mathbb{R}^3$, which is parametrized by slow-time $s \in \mathcal{L} := [0, T_{\text{obs}}]$. The observation time $T_{\text{obs}} \in \mathbb{R}_+$ corresponds to the synthetic aperture length $L_{\text{apt}} \in \mathbb{R}_+$. Periodically, chirp pulses [10]

$$p(t) = \text{rect}(\tfrac{t}{T}) \exp(-2\pi \mathrm{i} f_{\text{c}} t) \exp(\mathrm{i}\pi\kappa t^2) \tag{1}$$

for $t \in \mathbb{R}$ are transmitted by the antenna, where f_{c} is the carrier frequency, $\kappa = B/T$ the chirp rate, B the chirp bandwidth and T the pulse duration. This electromagnetic wave p is scattered at some objects on the ground or by the ground itself and reaches the antenna after a short period of time. The surface $\Omega \subset \mathbb{R}^3$, especially each $\boldsymbol{x} \in \Omega$, represents the topography of the underlying landscape and the reflectivity function $\mathcal{R} : \Omega \to \mathbb{C}$ describes how strong electromagnetic waves are reflected. Within the fast-time sampling interval $\mathcal{T}$ the receiver measures the recorded data

$$d_{\text{rec}}(t, s) = \int_\Omega A(\boldsymbol{x}, s)\, \mathcal{R}(\boldsymbol{x})\, p(t - 2/c \cdot || \boldsymbol{\gamma}(s) - \boldsymbol{x}||)\, \mathrm{d}\boldsymbol{x} \tag{2}$$

for $t \in \mathcal{T}$ and $s \in \mathcal{L}$, which consist of the superposition of multiple echos. Here, $2/c \cdot || \boldsymbol{\gamma}(s) - \boldsymbol{x}||$ is the two-way round-trip time between the antenna and the location $\boldsymbol{x} \in \Omega$, where c is the speed of light. Equation (2) is similar to the signal model given by Cheney [11]. The antenna footprint $A : \Omega \times \mathcal{L} \to \{0, 1\}$ is a binary function and indicates, depending on the slow-time, which area on the ground is illuminated by the antenna. In a spotlight scenario the scene is illuminated during the entire observation time, such that $A(\boldsymbol{x}, s) = 1$ holds for all $\boldsymbol{x} \in \Omega$ and all $s \in \mathcal{L}$. After d_{rec} is received, it is converted to baseband, which is mathematically described by the modulation

$$d_{\text{raw}}(t, s) = d_{\text{rec}}(t, s) \cdot \exp(2\pi \mathrm{i} f_{\text{c}} t). \tag{3}$$

The raw data d_{raw} is sampled with Nyquist rate and transferred to the digital SAR processor. It is matched filtered with the reference baseband chirp $p_{\text{ref}}(t) = \text{rect}(t/T) \exp(\mathrm{i}\pi\kappa t^2)$ with $t \in \mathcal{T}$ and results in the range-compressed data [10]

$$d(t, s) = d_{\text{raw}}(t, s) * p_{\text{ref}}^*(-t) \tag{4}$$

$$\approx \int_\Omega \mathcal{R}(\boldsymbol{x})\, \text{si}\big(\pi B(t - 2/c \cdot || \boldsymbol{\gamma}(s) - \boldsymbol{x}||)\big) \tag{5}$$

$$\cdot \exp(-4\pi \mathrm{i} f_{\text{c}}/c \cdot || \boldsymbol{\gamma}(s) - \boldsymbol{x}||)\, \mathrm{d}\boldsymbol{x}$$

for $t \in \mathcal{T}$ and $s \in \mathcal{L}$. The operation $*$ stands for the convolution and $(\cdot)^*$ is the complex conjugation. We implement the range compression according to (4). However, the stationary phase approximation [10] applied to (4) leads to a better understanding of the range-compressed data in terms of si-functions, visualized in (5).

3. Backprojection and State-of-the-Art Autofocus

The *global backprojection* (GBP) algorithm, invented by Andersson [7], is an image reconstruction technique to generate a SAR image from range-compressed data. The general idea of the GBP algorithm is the radially symmetrical projection of the measured range profiles $d_m(\cdot) := d(\cdot, s_m)$ from the discrete aperture positions $\boldsymbol{\gamma}_m := \boldsymbol{\gamma}(s_m)$ for $m = 1, \ldots, M$ back to a predefined $N \times N$ image grid on the ground. All N^2 pixels are represented by their center coordinates $\boldsymbol{x}_i \in \mathbb{R}^3$ for $i = 1, \ldots, N^2$ and all range profiles are sequentially processed and accumulated coherently in image-domain. The complex valued reflectivity $\mathcal{R}(\boldsymbol{x}_i)$ of a pixel at $\boldsymbol{x}_i$ is reconstructed by

$$\mathcal{R}(\boldsymbol{x}_i) = \sum_{m=1}^{M} \underbrace{d_m\big(2/c \cdot ||\boldsymbol{\gamma}_m - \boldsymbol{x}_i||\big) \, \exp\big(4\pi i f_c/c \cdot ||\boldsymbol{\gamma}_m - \boldsymbol{x}_i||\big)}_{=:\, b_m(\boldsymbol{\gamma}_m, \boldsymbol{x}_i)}, \tag{6}$$

where $b_m(\boldsymbol{\gamma}_m, \boldsymbol{x}_i)$ denotes the backprojected range profile in image-domain. We use linear interpolation to obtain the values $d_m(\cdot)$. The complex valued reflectivity image $\mathcal{R}$ is difficult to interpret. Thus, the image is often described by its real valued amplitude $\mathcal{A} = |\mathcal{R}|$ or its real valued intensity $\mathcal{I} = \mathcal{A}^2 = \mathcal{R} \cdot \mathcal{R}^*$, both visualized in decibel.

The knowledge of the true flight path $\boldsymbol{\gamma}$ is necessary for the reconstruction of a high quality SAR image. In reality, an INS measures the flight path $\widehat{\boldsymbol{\gamma}} = \boldsymbol{\gamma} + \boldsymbol{\gamma}^\epsilon$ with high precision. The *antenna position error* (APE) $\boldsymbol{\gamma}^\epsilon : \mathcal{L} \to \mathbb{R}^3$ denotes the measurement error of the INS and is the main reason for a smeared image, smeared in azimuth direction. If the measured flight path $\widehat{\boldsymbol{\gamma}}_m := \widehat{\boldsymbol{\gamma}}(s_m)$ and the APE $\boldsymbol{\gamma}_m^\epsilon := \boldsymbol{\gamma}^\epsilon(s_m)$ would be available for all $m = 1, \ldots, M$, a sharp image could theoretically be reconstructed by

$$\mathcal{R}(\boldsymbol{x}_i) = \sum_{m=1}^{M} d_m\big(2/c \cdot ||\widehat{\boldsymbol{\gamma}}_m - \boldsymbol{x}_i|| - 2/c \cdot r_m^\epsilon(\boldsymbol{x}_i)\big)$$
$$\cdot \exp\big(4\pi i f_c/c \cdot ||\widehat{\boldsymbol{\gamma}}_m - \boldsymbol{x}_i||\big) \cdot \exp\big(-4\pi i f_c/c \cdot r_m^\epsilon(\boldsymbol{x}_i)\big), \tag{7}$$

where the range errors r_m^ϵ are defined as

$$r_m^\epsilon(\boldsymbol{x}_i) := ||\widehat{\boldsymbol{\gamma}}_m - \boldsymbol{x}_i|| - ||\widehat{\boldsymbol{\gamma}}_m - \boldsymbol{\gamma}_m^\epsilon - \boldsymbol{x}_i|| \tag{8}$$

for $m = 1, \ldots, M$ and $i = 1, \ldots, N^2$. In reality, the APEs $\boldsymbol{\gamma}_m^\epsilon \in \mathbb{R}^3$ and thus the range errors $r_m^\epsilon(\boldsymbol{x}_i) \in \mathbb{R}$ for all $m = 1, \ldots, M$ and all $i = 1, \ldots, N^2$ are unknown and difficult to estimate. Nevertheless, in order to run an autofocus algorithm despite of the unknown range errors, most state-of-the-art techniques simplify (7) by using the following assumptions: They firstly assume that the range errors do not depend on space, i.e., on pixel location $\boldsymbol{x}_i$, such that $r_m^\epsilon(\boldsymbol{x}_i) \approx r_m^\epsilon$ holds for all $m = 1, \ldots, M$ and all $i = 1, \ldots, N^2$. This approximation is true in most far-field scenarios. They additionally assume that all range errors r_m^ϵ are less than one half of the range resolution δ_r for all $m = 1, \ldots, M$, which is true, if the measured flight path $\widehat{\boldsymbol{\gamma}}$ is measured with high precision and thus a good estimate of $\boldsymbol{\gamma}$. Hence, by assuming $r_m^\epsilon(\boldsymbol{x}_i) \approx r_m^\epsilon$ and $r_m^\epsilon \leq \delta_r/2$

for all $m = 1, \ldots, M$ and all $i = 1, \ldots, N^2$, Equation (7) can be approximated by

$$\mathcal{R}(\boldsymbol{x}_i) \approx \sum_{m=1}^{M} b_m(\widehat{\boldsymbol{\gamma}}_m, \boldsymbol{x}_i) \, \exp\big(- \mathrm{i} \, \phi_m^\epsilon\big), \tag{9}$$

where the phase correction term

$$\phi_m^\epsilon = \frac{4\pi f_\mathrm{c}}{c} \cdot r_m^\epsilon \tag{10}$$

is used for small r_m^ϵ to generate a focused SAR image. Equation (9) shows implicitly that in the case of an inaccurately measured flight path, the original backprojected data $b_m(\boldsymbol{\gamma}_m, \boldsymbol{x}_i)$ becomes phase corrupted $b_m(\widehat{\boldsymbol{\gamma}}_m, \boldsymbol{x}_i) = b_m(\boldsymbol{\gamma}_m, \boldsymbol{x}_i) \exp(\mathrm{i} \, \phi_m^\epsilon)$ for all $m = 1, \ldots, M$ and all $i = 1, \ldots, N^2$. The task of traditional autofocus techniques is to estimate the unknown phase errors $\phi_m^\epsilon \in (-\pi, \pi]$ and to correct the phase corrupted data automatically. In addition, varying atmospheric propagation delays, imperfections of several hardware components and phase noise result in radar system timing errors [1]. These timing errors can also be modeled as independent phase errors ϕ_m^ϵ and thus are corrected by autofocus techniques without additional adjustments.

State-of-the-Art Autofocus Algorithm by Ash

One of the most common time-domain autofocus techniques is the backprojection autofocus by Ash [9]. He estimates one phase error $\phi_m^\epsilon \in (-\pi, \pi]$ per pulse by maximizing image sharpness. To compute all phase errors for $m = 1, \ldots, M$ he uses a coordinate descent framework, where each ϕ_m^ϵ is optimized separately. During a single turn, one ϕ_m^ϵ is optimized, while the others stay fixed. This procedure can be done a few times to compensate dependencies between the phase errors. In each turn, considering an arbitrary m, the algorithm solves the non-linear least square problem

$$\widehat{\phi}_m^\epsilon = \underset{\phi_m^\epsilon \in (-\pi, \pi]}{\arg\max} \, S(\phi_m^\epsilon) \tag{11}$$

where $S : (-\pi, \pi] \to \mathbb{R}_+$ is the image sharpness cost function

$$S(\phi_m^\epsilon) = \sum_{i=1}^{N^2} ||\mathcal{R}(\boldsymbol{x}_i, \phi_m^\epsilon)\mathcal{R}^*(\boldsymbol{x}_i, \phi_m^\epsilon)||^2. \tag{12}$$

This metric works well in autofocus frameworks on a variety of scene types [12]. Ash [9] was able to formulate a closed-form solution of (11), which improves not only the precision of the estimation, but also the computational time. Details can be found in his work [9]. If the phase error $\widehat{\phi}_m^\epsilon$ for a fixed m has been successfully estimated, the reflectivity image can be updated using (9) and m can be incremented. In summary, the algorithm begins with the unfocused SAR image reconstructed by the GBP algorithm and subtracts the first backprojected pulse b_1 from the image. Then, the first phase error $\widehat{\phi}_1^\epsilon$ is estimated by solving (11). Afterwards, the subtracted pulse b_1 is phase corrected and added coherently back to the image. The next backprojected pulse b_2 can be considered.

4. Proposed Autofocus

Our autofocus approach estimates pulse-by-pulse the phase errors by maximizing image sharpness similar to the backprojection autofocus by Ash [9]. We propose to use the estimated phase error of the currently considered pulse to correct all subsequent aperture positions such that the rest of the flight path is updated. This error propagation is our main adjustment to the algorithm, which eliminates the limitation of a maximal correctable antenna position error of approximately one half of the range resolution. An overview of our algorithm is visualized in the flow-chart Figure 1.

Figure 1: Overview flow-chart of proposed autofocus algorithm.

In the following, we describe our method in detail. In the preprocessing, we divide the observation time interval $\mathcal{L}$ into two parts. The first part is used to generate an initial SAR image $\mathcal{R}_0$ by the standard GBP algorithm. This image serves as a registration basis for all following pulses. The first time interval should be very short, for example $50\,\mathrm{ms}$, since the entire autofocus works best, if within this short time interval the true flight path is approximately a straight line. The second part of $\mathcal{L}$ is used to estimate pulse-by-pulse all phase errors by maximizing image sharpness, such that the sequentially corrected pulses fit perfectly to the initial image $\mathcal{R}_0$. Only this second part is visualized in Figure 1. We begin with the initial image $\mathcal{R}_0$, take the next backprojected pulse and estimate one phase error $\widehat{\phi}_m^\epsilon$ for a fixed slow-time sample m by solving (11) using the Ash [9] method. This phase error is used to correct the phase of the currently considered backprojected pulse b_m, before it is coherently added to the image. The same estimated phase error $\widehat{\phi}_m^\epsilon$ is additionally converted to a range error

$$\Delta \widehat{r}_m^\epsilon = \frac{c}{4\pi f_\mathrm{c}} \cdot \widehat{\phi}_m^\epsilon, \tag{13}$$

which describes the differential range error from pulse to pulse. This differential range error is used to update the distance from the subsequent aperture position to all pixels, compare (8), by

$$r_{m+1}^\epsilon = r_m^\epsilon + \Delta \widehat{r}_m^\epsilon. \tag{14}$$

This is equivalent to adjust the subsequent aperture position $\widehat{\gamma}_{m+1}$ before considering the next pulse. The error propagation of the range error to all subsequent aperture positions allows us to correct much larger antenna position errors than state-of-the-art algorithms. Since from pulse to

pulse an antenna position error of maximal one half of the wavelength can be reliably estimated without phase wrapping effects, our theoretical maximal correctable deviation to the true flight path is

$$r_{\max}(s) = \frac{\lambda \, f_{\mathrm{prf}}}{2} \cdot s, \tag{15}$$

which is for $\lambda = 3\,\mathrm{cm}$ and $f_{\mathrm{prf}} = 2\,000\,\mathrm{Hz}$ approximately $30\,\mathrm{m/s}$ in range direction. In contrast to our method, the backprojection autofocus by Ash [9] needs the finally reconstructed smeared SAR image. The autofocus uses a coordinate descent iteration such that each pulse must again be computed, subtracted from the image, phase corrected and added back to the image. Thus, it needs roughly two times the computational load of the GBP algorithm. Since our autofocus is integrated into the GBP algorithm, we do not need a coordinate descent iteration, which reduces computational costs. Thus, we have only the additional costs of the phase estimated and range correction, which is much less than the costs of the GBP. Hence, our algorithm is much faster than the Ash autofocus. The proposed method can easily be adopted to other bands like L-band.

5. Experimental Results

We use the real experimental data of the public Gotcha data set published by Scarborough [2] to evaluate our autofocus algorithm. We compare our results with the results of the original state-of-the-art backprojection autofocus by Ash [9]. The used data set [2] contains measurements of an airborne single-channel X-band SAR system with a chirp bandwidth of $640\,\mathrm{MHz}$ and a corresponding range resolution of $24\,\mathrm{cm}$. It was measured along a circle segment and provides data from a narrow strip to reduce the amount of data stored in one file. The system observed an area of Dayton City in Ohio, USA. Some characteristic parameters of the data set [2] are given in Table 1. The data set contains the original flight path, such that a perfect image can be reconstructed without the usage of an autofocus technique.

Table 1: Parameters of public Gotcha data set [2] and SAR geometry.

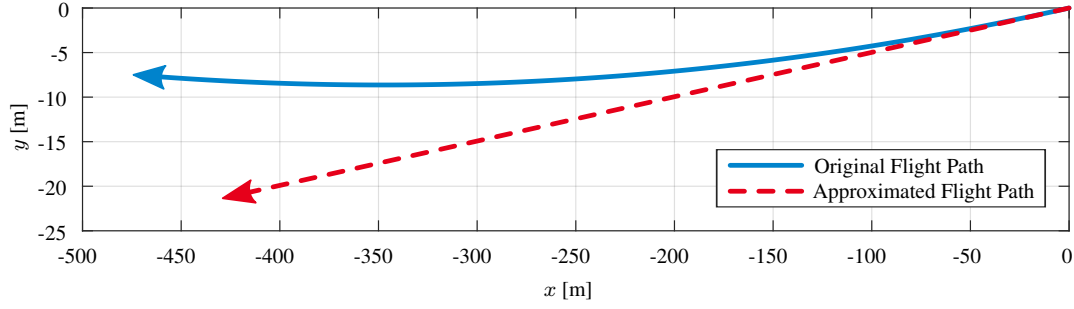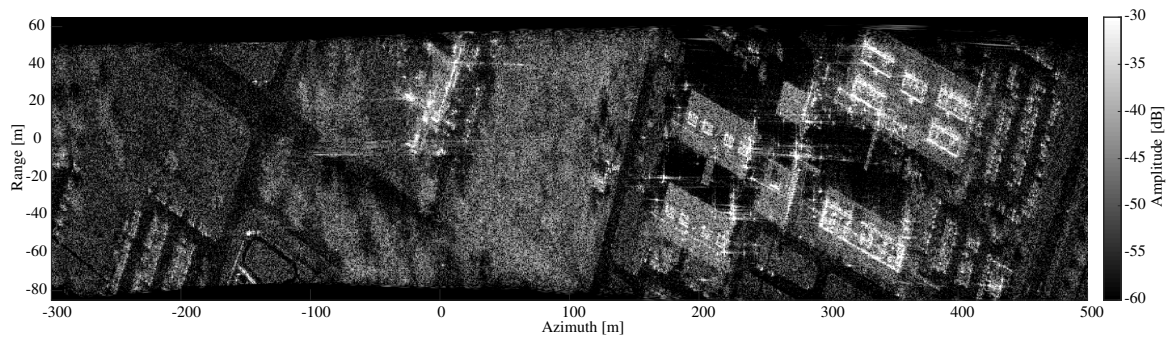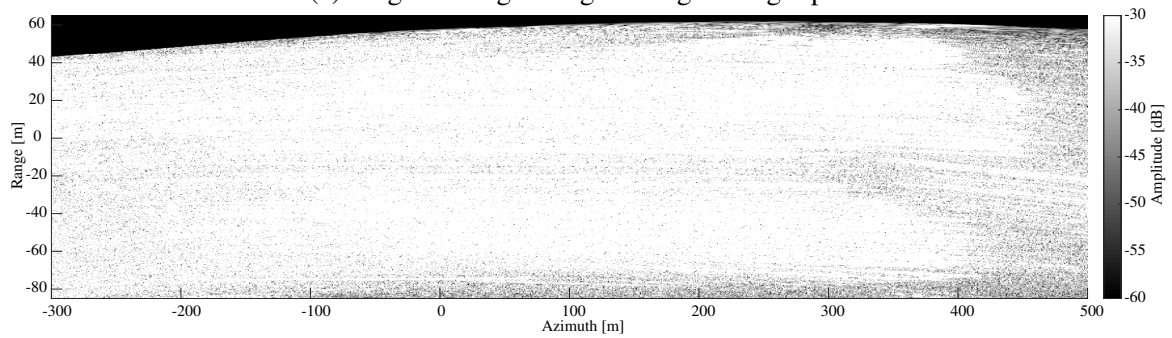| Parameter	Value
Carrier Frequency f_{c}	$9.6\,\mathrm{GHz}$
Wavelength λ	$3.3\,\mathrm{cm}$
Chirp Bandwidth B	$640\,\mathrm{MHz}$
Range Resolution δ_r	$23\,\mathrm{cm}$
Pulse Duration T	$30\,\mu\mathrm{s}$
Pulse Repetition Frequency f_{prf}	$2\,170\,\mathrm{Hz}$
Squint Angle θ_{s}	$0°$
Depression Angle θ_{d}	$44.9°$
Slant Range r_0	$10\,\mathrm{km}$
Observation Time T_{ops}	$4\,\mathrm{s}$
Aircraft Speed v_0	$110\,\mathrm{m/s}$

Figure 2: Original (blue solid) and approximated (red dashed) flight path. The maximal antenna position error is more than $12\,\text{m}$ in y-direction.
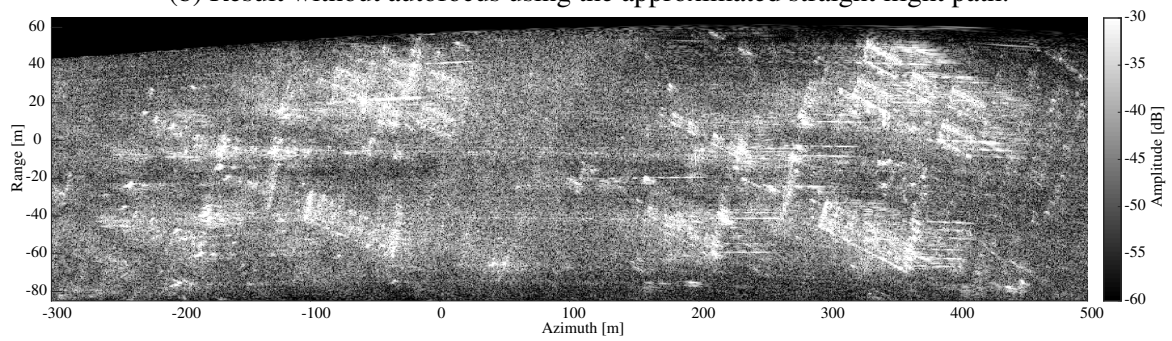
To show the effectiveness of our autofocus algorithm, we generate a coarsely approximated flight path from the original flight path only by using the aircraft speed and the flight direction at the beginning of the observation time. We obtain a straight line, visualized as red dashed line in Figure 2, which is only similar to the true flight path, depicted as blue solid curve in Figure 2, at the beginning of the flight. After $4\,\text{s}$ the deviation to the original flight path is more than $12\,\text{m}$ in range direction, here y-direction. We initialize the GBP reconstruction by an image grid of $1\,000 \times 500$ pixels, where each pixels has a spacing of $80 \times 30\,\text{cm}$. We process $8\,192$ pulses from an observation time of $4\,\text{s}$ and use the data from the first $50\,\text{ms}$ to reconstruct the initial image $\mathcal{R}_0$, before we start our integrated autofocus, explained in Section 4. The original image, reconstructed from the real data and the original flight path, is shown in Figure 3 (a). Some buildings, some streets and some parking cars can clearly be seen in the focused image. This original image is the reference image. Using the approximated flight path instead of the true one, both visualized in Figure 2, without any autofocus results in Figure 3 (b). This image is totally smeared and useless for image interpretation tasks. The results of the GBP algorithm in combination with the backprojection autofocus by Ash [9] using the approximated flight path is shown in Figure 3 (c). One can guess that some buildings could be in the image. However, some of these buildings are ghost buildings caused by ambiguities such that this image cannot be used for a reliably interpretation. The reason is that the assumption of an maximal antenna position error of one half of the range resolution equal to $12\,\text{cm}$ does not hold in this scenario. Our proposed autofocus algorithm leads to the image presented in Figure 3 (d). From a visual point of view, the image is as good as the original image. However, some parts on the left side and on the right side of the image are slightly smeared. Additionally, the entire image is shifted in azimuth and scaled, such that not all details at the image border in Figure 3 (a) can be seen in Figure 3 (d). The reason is that the approximated flight path in the first $50\,\text{ms}$ has a slightly different direction and a slightly different curvature than the original flight path. This shifts and scales the image. In summary, our reconstructed image in Figure 3 (d) is much better focused than the image in Figure 3 (c) coming from the state-of-the-art backprojection autofocus by Ash [9]. The total costs of the GBP algorithm, which is implemented in Matlab on the basis of Gorham's implementation [8], are $5\,\text{min}$ and $20\,\text{s}$ on a work station with a $3.5\,\text{GHz}$ Quad-Core processor and $32\,\text{GB}$ RAM. The Ash autofocus needs $11\,\text{min}$ and $30\,\text{s}$ resulting in the entire costs of $16\,\text{min}$ and $50\,\text{s}$. Our proposed autofocus is much faster and needs only $3\,\text{min}$.
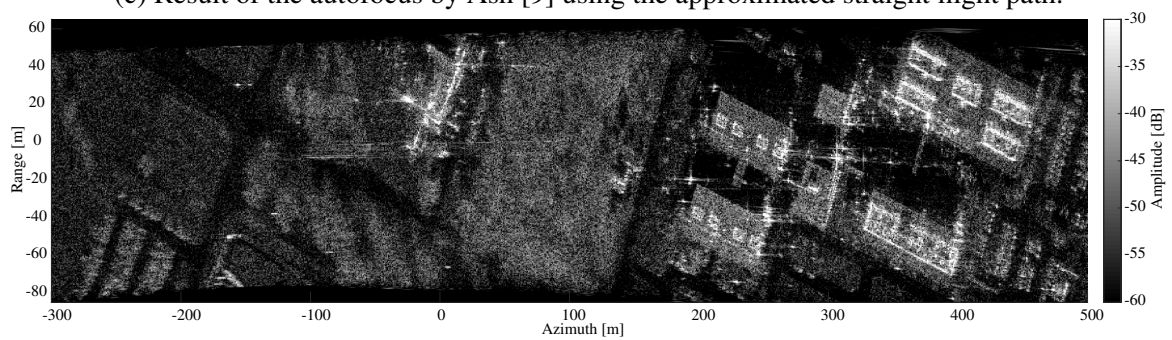
8

(a) Original image using the original flight path.

(b) Result without autofocus using the approximated straight flight path.

(c) Result of the autofocus by Ash [9] using the approximated straight flight path.

(d) Result of our proposed autofocus using the approximated straight flight path.

Figure 3: Reconstructed SAR images from the Gotcha data set [2]. In (a) the original flight path is used to reconstruct the original image. In (b)–(c) the approximated straight flight path is used.

6. Conclusions

We presented an extended autofocus technique for backprojection, which generates sharp SAR images even if only the coarse speed and the coarse flight direction of the aircraft instead of very precise INS measurements are available. Our algorithm uses the idea of the backprojection autofocus by Ash [9] and estimates pulse-by-pulse the phase errors by maximizing image sharpness. We extended this algorithm and propose to use the estimated phase error of the currently considered pulse to correct all following aperture positions and thus the flight path of the aircraft. This error propagation enables the reconstruction of focused SAR images as long as the antenna position errors are less than one half of the wavelength from pulse to pulse, which is much more than the upper bound of state-of-the-art autofocus techniques. The effectiveness of the proposed autofocus algorithm was proven by real experimental data from an airborne single-channel X-band system [2]. The results show that our algorithm is able to estimate antenna position errors of more than $12\,\mathrm{m}$, where the Ash [9] autofocus results in unrecognizable images. Hence, using our proposed algorithm enables the usage of a simpler INS system or even no INS system, which reduces costs and weight of the radar system immensely. This will be very important for example in the case of UAV SAR.

References

[1] M. I. Duersch and D. G. Long, "Backprojection Autofocus for Synthetic Aperture Radar", *Department of Electrical and Computer Engineering*, Brigham Young University, 2013.

[2] S. M. Scarborough, C. H. Casteel, L. Gorham, M. J. Minardi, U. K. Majumder, M. G. Judge, E. Zelnio, M. Bryant, H. Nichols and D. Page, "A challenge problem for SAR-based GMTI in urban environments", *Proc. SPIE*, Vol. 7337, pp. 7337-7347, 2009.

[3] P. H. Eichel, D. C. Ghiglia and C. V. Jakowatz, Jr., "Speckle Processing Method for Synthetic Aperture Radar Phase Correction", *Optics Letters*, vol. 14, no. 1, January 1989.

[4] M. P. Nguyen, "Bewegungskompensation und Autofokussierung von SAR-Rohdaten mit großem Schielwinkel", *VDI Verlag*, Fortschr.-Ber. VDI Reihe 10, 2014.

[5] C. E. Mancill and J. M. Swiger, "A Mapdrift Autofocus Technique for Correcting Higher Order SAR Phase Errors", *27th Annual Tri-Service Radar Symposium Record*, Monterey, CA, pp. 391-400, 1981.

[6] W. G. Carrara, R. S. Goodman and R. M. Majewski, "Spotlight Synthetic Aperture Radar: Signal Processing Algorithms", *Boston: Artech House*, 1995.

[7] L. E. Andersson, "On determination of a function from spherical averages", *SIAM Journal on Mathematical Analysis*, vol. 19, pp. 214–341, 1988.

[8] L. A. Gorham and L. J. Moore, "SAR image formation toolbox for MATLAB", *Proc. SPIE*, Vol. 7699, Algorithms for Synthetic Aperture Radar, Imagery XVII, 2010.

[9] J. N. Ash, "An Autofocus Method for Backprojection Imagery in Synthetic Aperture Radar", *IEEE Geoscience and Remote Sensing Letters*, pp. 104-108, January 2012.

[10] I. A. Cumming, F. H. Wong "Digital Processing of Synthetic Aperture Radar Data - Algorithms and Implementation", *Artech House*, Boston, 2005.

[11] M. Cheney and B. Borden "Fundamentals of Radar Imaging", *SIAM*, Philadelphia, 2009.

[12] J. R. Fienup and J. J. Miller, "Aberration correction by maximizing generalized sharpness metrics", *J. Opt. Soc. Amer. A., Opt. Image Sci.*, vol. 20, no. 4, pp. 609–620, Apr. 2003.